JOURNAL OF MATERIALS SCIENCE 27 (1992) 5483–5496

Experimental characterization of the tensile behaviour of Nicalon fibre-reinforced calcium aluminosilicate composites

S-W. WANG*, A. PARVIZI-MAJIDI
Center for Composite Materials, Department of Mechanical Engineering and Materials Science Program, University of Delaware, Newark, DE 19716, USA

Mechanical behaviour studies were conducted on Nicalon SiC/calcium aluminosilicate (CAS) composites. Tensile tests were carried out to study the stress–strain behaviour, as well as to identify the failure mechanisms, of unidirectional and cross-ply SiC/CAS composites. The evolution of the various damage modes and the synergistic effects among them were investigated. The effect of the 90° ply thickness on the damage modes was also determined. The composite stiffness reduction during damage evolution was evaluated. A tensile test specimen was designed for glass and glass-ceramic composites to avoid end-tab shear failure and expensive machining as well as to reduce the effect of bending due to misalignment. The results of this work provide insight into the stress–strain behaviour and damage mechanisms of continuous fibre-reinforced ceramic composites which can be very valuable in design with these materials.

1. Introduction

Ceramic matrix composites have received increasing attention during the last decade. Their low density, improved toughness compared to the monolithic ceramics, and high-temperature capability have made them promising candidates for high-temperature structural application [1, 2]. However, the mechanical behaviour of these composites, in which the fibre has a larger strain to failure than the matrix, usually involves extensive damage prior to the ultimate failure. Damage in the well-studied unidirectional fibre-reinforced composites is in the form of regularly spaced cracks in the matrix. This multiple matrix microcracking has been observed in many materials systems [3–5] and was first treated by Aveston *et al.* [6, 7].

Multi-directional composite laminates exhibit a more complex damage behaviour. Failure mechanisms in cross-ply and angle-ply laminates have been studied for fibre-reinforced polymer matrix composites. Transverse cracking and free-edge delamination are the two major types of damages in these composites.

Transverse cracks form in laminates where a sufficiently large tensile stress exists normal to the fibres as illustrated in Fig. 1 for a $(0/90)_s$ cross-ply laminate. Garrett and Bailey [8] applied the multiple cracking theory of Aveston and Kelly [7] to the problem of transverse cracking in 0,90,0 cross-ply glass fibre-reinforced plastics. They found that, similar to the matrix cracks in unidirectional composites, transverse cracks in the 90° ply showed a remarkably even spacing which depended on both the ply thickness and the applied stress; the higher the applied stress and the smaller the 90° ply thickness, the smaller the average crack spacing. Parvizi and co-workers [9, 10] extended the studies of transverse cracking to glass/epoxy and graphite/epoxy cross-ply laminates and noted the effect of the transverse ply thickness on the strain for the onset of cracking. They demonstrated both experimentally and from an energy approach that transverse cracking initiates at an increasingly larger strain with decreasing 90° ply thickness and it could be even completely suppressed at sufficiently small ply thicknesses. They also treated the effects of the Poisson's contraction and residual thermal stresses and investigated longitudinal cracking of the 0° plies due to those effects.

Free-edge delamination is generally associated with the out-of-plane normal or shearing stresses (Fig. 2). Elastic analyses have shown that stresses of high gradient can be induced near the free edges of laminates by mechanical, thermal or hygroscopic loadings [11–13]. The magnitude and nature of these stresses depend greatly on the specimen geometry, ply stacking sequence and ply properties besides the applied load. In many cases, the location of the observed

* *Present address*: Advanced Metallic and Ceramic Materials Branch, Code 6063, Naval Air Development Center, Warminster, PA 18974, USA.

0022–2461

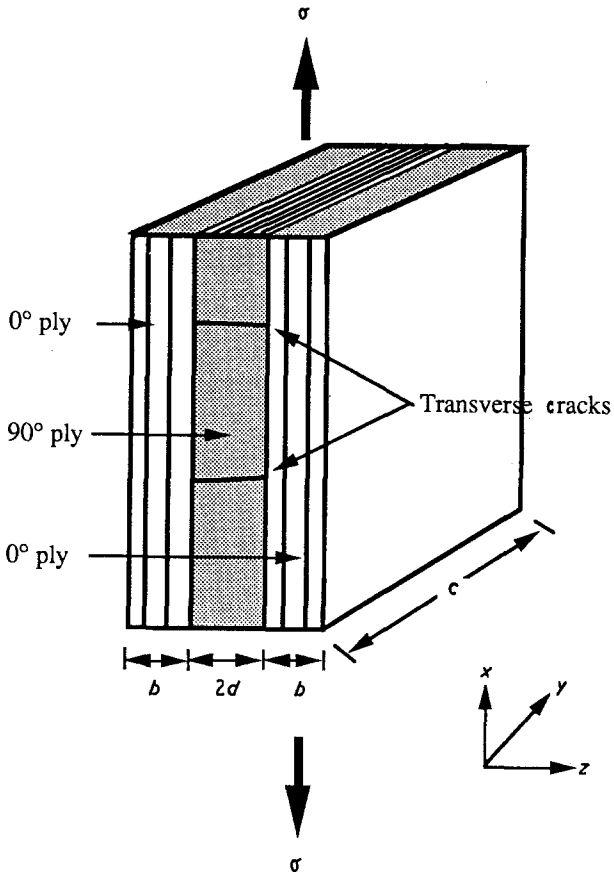

Figure 1 Schematic view of transverse cracks in 0,90,0 cross-ply laminate under uniaxial loading.

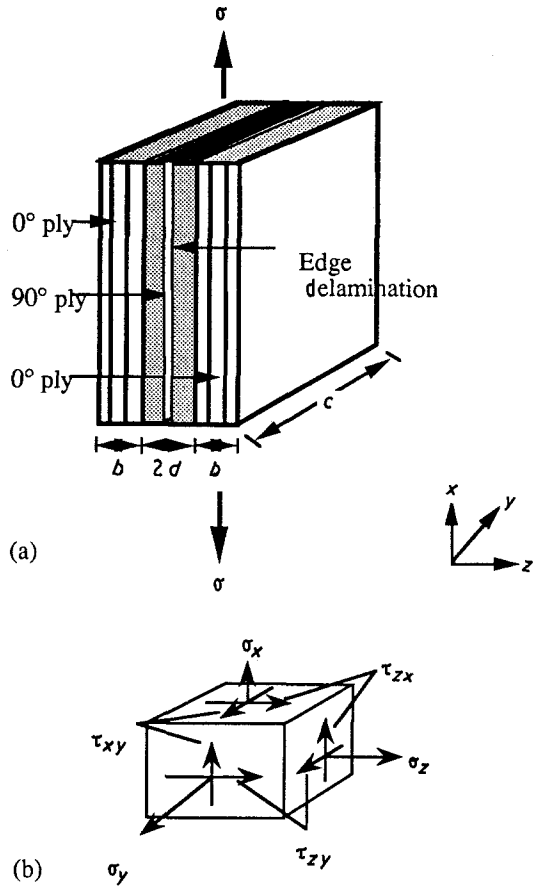

Figure 2 (a) Schematic view of an edge delamination in a 0,90,0 cross-ply laminate under uniaxial loading, and (b) the associated stress components.

delamination can be predicted from the calculated free-edge stresses [14]. However, in other cases, delamination does not occur even when the calculated edge stresses are several times larger than the expected material strength. A theoretical approach which unifies the basic concept of fracture mechanics with that of statistical material effective flaws has been developed by Wang and Crossman [15] to solve the problem. The introduction of material effective flaws is an attempt to account for the sources of material weakness and the random nature of their existence while the use of fracture mechanics provides the necessary criterion for the propagation behaviour of the flaws. By calculating the strain energy release rate of a crack at each possible location and comparing it to the property of the laminate, predictions can be made concerning the likelihood of crack propagation at a given location and its onset strain. Successful correlations of this analytical solution with the experimental results have been demonstrated [16, 17].

In fibre-reinforced ceramic matrix composites, in addition to the transverse cracking and delamination modes of failure, matrix microcracking in the 0° plies is expected to occur because of the brittle nature of the ceramic matrix. All these damage modes which occur before the ultimate failure are of prime concern from a design standpoint because they signify the onset of permanent damage and the loss of integrity. In this study, tensile behaviour of unidirectional and 0,90,0 cross-ply laminates of Nicalon fibre-reinforced calcium aluminosilicate (CAS) were investigated. The objective was to provide a systematic characterization of (i) the evolution and mechanisms of damage, (ii) the possible synergisms amongst the various damage modes, and (iii) the effect of damage on composite properties such as stiffness.

A special technique for preparing tensile test coupons is presented here. This technique which involves casting integrated epoxy end tabs was developed especially for fibre-reinforced glass and glass-ceramic matrix composites in order to reduce bending and to facilitate the *in situ* observation of the microstructural changes during testing.

2. Experimental procedure

2.1. Materials

The composite laminates of Nicalon fibre-reinforced calcium aluminosilicate were produced by a slurry infiltration/hot pressing process followed by a ceraming heat treatment. The unidirectional composite was made of eight plies. The 0,90,0 cross-ply laminates were made with three outer 0° plies on each side and varying number of inner 90° plies (from one to three layers). Fibre volume fraction was 0.36 ± 0.02 in all composites. Properties of the CAS matrix and the Nicalon fibres are listed in Table I.

2.2. Tensile tests

Tensile tests were conducted at room temperature on both unidirectional and cross-ply SiC/CAS laminates.

TABLE I Characteristics of matrix and fibres in the SiC/CAS composites

Properties	CAS matrix[a]	Nicalon[b] SiC Fibres
Elastic modulus (GPa)	98	193.2
Tensile strength (MPa)	124 (flexural)	2760
Poisson's ratio	0.255	–
Coefficient of thermal expansion ($°C^{-1}$)	5.0×10^{-6}[c]	4.0×10^{-6}[d]
Density ($g\,cm^{-3}$)	2.76	2.55
Fibre diameter (μm)	–	10–20
Fracture toughness ($MPa\,m^{1/2}$)	2.2	2.3
Maximum Use Temperature (°C)	1350	1300
Crystalline phase	Anorthite	β-SiC

[a] From Corning, Inc.
[b] From Dow Corning Co..
[c] 0–900 °C.
[d] 0–1000 °C.

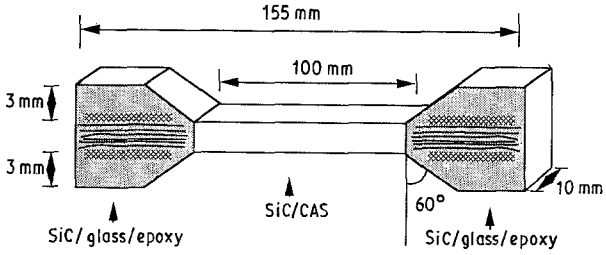

Figure 3 End-tabbed tensile specimen.

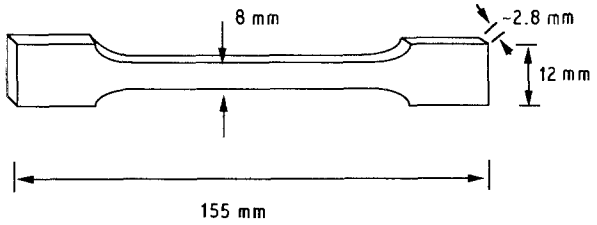

Figure 4 Tensile test specimen with narrowed gauge section.

For unidirectional laminates, the specimens were tested with the fibre axis parallel to the applied load. For 0,90,0 cross-ply laminates, the applied load was aligned with the fibre axis in the outer, 0° plies.

To avoid end-tab shear failure, reduce bending from minor misalignments, and facilitate the *in situ* monitoring of the microstructure, a test coupon with integrated end tabs was designed for this study. To prepare the test coupon, a rectangular strip of the composite, 155 mm × 10 mm × 2.8 mm, was first cut from the panel with a diamond saw. The calcium aluminosilicate matrix along a 25 mm length at each end of the strip was removed by soaking the ends in a 40% solution of hydrofluoric acid for 24 h, leaving the SiC fibres exposed. After cleaning with acetone and drying, the composite strip with the loose SiC fibres hanging from its ends was placed in an aluminium mould. The mould had been sprayed with a release agent in order to facilitate subsequent removal of the specimen. Four layers of a plain weave glass fibre fabric were placed above and below the loose SiC fibres at each end to provide further reinforcement at the end tabs. For cross-ply laminates, layers of glass fabric were also inserted between the 0° plies to replace the fallen 90° plies. The specimen ends were then cast in an epoxy resin (EPO-KWICK resin 20-8136-128 and hardener 20-8138-33) and cured at 50 °C for 2 h. After removal from the mould, the end tabs were lightly machined to the final dimension. A schematic representation of the finished specimen is shown in Fig. 3. One edge of the test coupons was then polished with diamond paste to a 1 μm finish to allow *in situ* observation of the microstructure during tensile testing.

The specimens were tested on an Instron machine Model 1125 at a crosshead speed of $1.27\,mm\,min^{-1}$. 0° and 0°/90° strain gauges were mounted on the opposite sides of each specimen to monitor the axial and transverse strains and to check for the presence of bending due to misalignment.

During testing, replicas were made from the polished edge at regular intervals of strain by pressing acetone-softened acetate tape against the specimen surface. When the tape hardened it provided a permanent record of surface details at the specimen edge. The polished surface had been slightly etched by 5% hydrofluoric acid in order to enhance the transfer of microstructural details on to replicas. The spacings between the matrix microcracks as well as the transverse cracks were subsequently measured from replicas under an optical microscope. The replication method was supplemented by *in situ* optical microscopy of the specimen edge.

For comparison, tensile tests were also conducted on untabbed coupons with reduced gauge section as depicted in Fig. 4. These specimens were tested at E. I. Du Pont de Nemours and Company, using an Instron Model 8652 which had been especially aligned to eliminate bending. For these specimens, the strain was measured using an extensometer with a 25.4 mm gauge length.

In addition to the monotonic tensile tests, a series of incremental load/unload/reload tests was carried out to investigate the evolution of damage and the associated changes in the elastic moduli of the unidirectional and cross-ply laminates. A specimen was repeatedly loaded to a certain strain, unloaded and then reloaded to a higher strain level. Elastic modulus was determined from the initial linear region of each loading cycle.

2.3. Fracture toughness measurements

The fracture toughness of the unidirectional laminates in the transverse direction (crack running parallel to the fibres) was determined using chevron-notched four-point bend specimens. The specimens were 50 mm long rectangular bars with cross-sectional dimensions close to 4 mm × 7 mm. A chevron notch was machined into these specimens with a 153 μm thick diamond blade. Specimens were loaded in a four-point bending fixture with the major and minor spans being 40 and 20 mm, respectively. The test fixture was designed to allow the support rollers and load rollers to

roll freely as the specimen was loaded. A cone-shaped loading head transmitted the load uniformly to the load rollers, and then to the specimen. The notch angle was 31°.

The specimens were fractured on an Instron model 1125 machine at a crosshead speed of 0.005 mm min^{-1}. Load was recorded as a function of load-point displacement. The maximum load, P_{max}, was obtained and the critical stress intensity factor, K_c was calculated using the slice model of Bluhm [18, 19]. The fracture surface energy, γ_t, was then calculated using the following equation

$$G_c = 2\gamma_t = \frac{K_c^2(1 - \nu_t^2)}{E_t}$$

where ν_t and E_t are the Poisson's ratio and the Young's modulus of the composite in the transverse direction, respectively.

2.4. Thermomechanical analysis

Thermomechanical analyses were performed on unidirectional laminates to determine the thermal expansion coefficients along the fibre direction as well as the transverse direction. Specimens were cut with parallel surfaces in the direction along which the dimension change was to be measured. The measurements were made with a Du Pont 9900 thermomechanical analyser, using a ramp rate of 5 °C min^{-1} from room temperature to 900 °C.

3. Results

3.1. Tensile stress–strain behaviour

Fig. 5 shows the tensile stress–strain curves for unidirectional and cross-ply laminates for both specimens with reduced gauge section and those with integrated end tabs. The correlation between the two specimen geometries is reasonably good, particularly for the cross-ply laminates. In fact, in most cases the end-tabbed specimens exhibited a larger strain-to-failure than the reduced-gauged specimens tested on well-aligned equipment. The stress–strain curves obtained on the end-tabbed specimens were very reproducible as shown in Fig. 6. All end-tabbed specimens failed within the gauge section (Fig. 7). This end-tabbing technique not only eliminated the problems of end-tab failure and reduced bending, it also made polishing and real-time microstructural monitoring at the specimen edge much easier.

For the unidirectional composite, the Young's modulus along the fibre direction, E_1, and Poisson's ratio, ν_1, were measured from the initial linear region and the values obtained were 131 GPa, and 0.29, respectively. The elastic modulus agrees well with that predicted from the rule of mixtures, which is 132 GPa.

From the optical microscopic observations, the matrix started to crack at an axial strain of about 0.13%. The first isolated matrix cracks usually appeared in the matrix-rich regions of the composite. The cracks, once initiated, stopped at the neighbouring fibres and subsequently propagated through the entire width of the specimen in a steady-state fashion as the applied load increased. These matrix microcracks were spaced quite evenly and eventually filled the entire matrix with a characteristic spacing. Fig. 8 shows the crack spacing measured from replica tapes as a function of strain. A mean crack spacing of 105 μm was obtained at failure.

The 0°,90°,0° cross-ply laminates exhibited several failure events during the tensile loading, including transverse cracking in the 90° ply, delamination cracking in the 90° ply, and matrix microcracking in the 0° plies. The onset strains for these failure events are listed in Table II.

Micrographs from replica tapes in Fig. 9 show the sequence of the failure events in the three cross-ply laminates tested. The transverse cracks occurred first, always initiating at the 0°/90° ply interface (Fig. 10). These cracks then propagated through the full width of the 90° ply. The strain for the onset of transverse cracking increased, and the crack propagation rate decreased, as the transverse ply thickness decreased (Table II). In the $0°_3/90°_3/0°_3$ laminate cracks, once

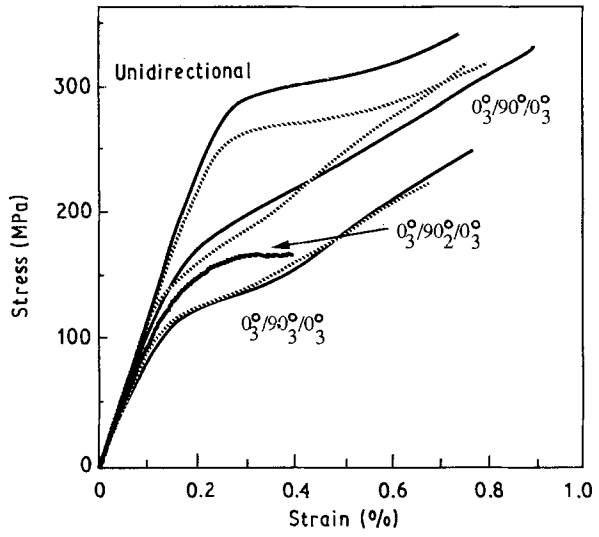

Figure 5 Tensile stress–strain curves for SiC/CAS unidirectional and cross-ply laminates.

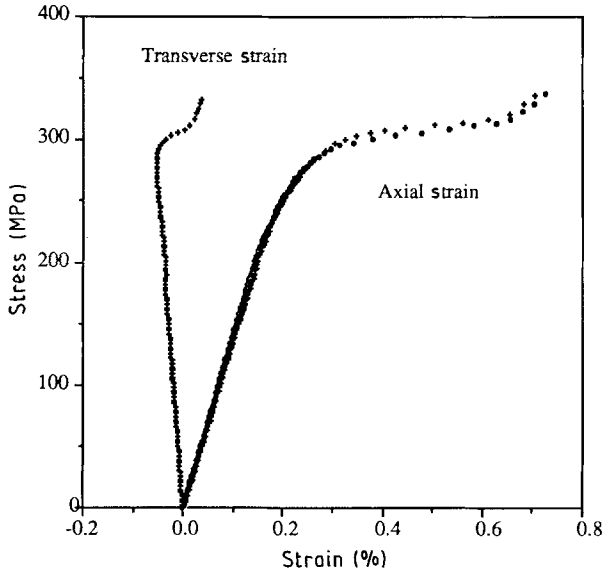

Figure 6 Tensile stress–strain curves for SiC/CAS unidirectional composite.

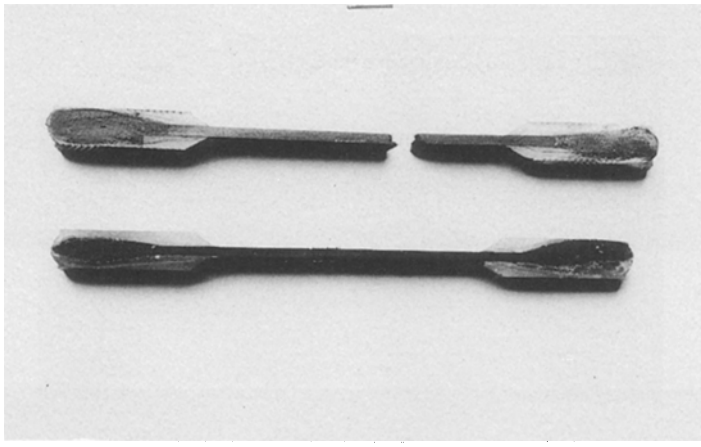

Figure 7 Specimens with the specially designed end tabs before and after the tensile tests.

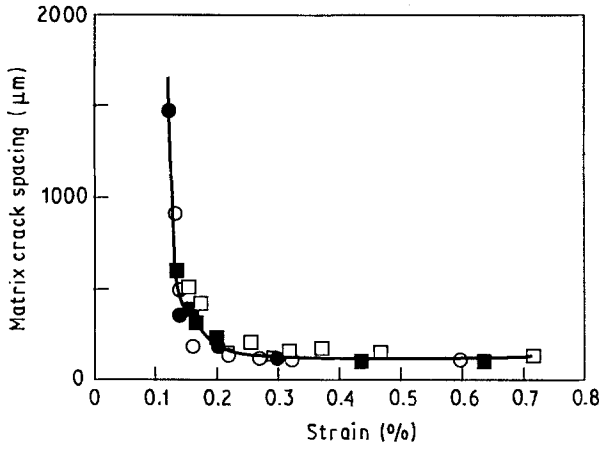

Figure 8 Average matrix crack spacing of SiC/CAS cross-ply laminates as a function of composite strain. (■) $0°_3/90°/0°_3$, (●) $0°_3/90°_2/0°_3$, (□) $0°_3/90°_3/0°_3$, (○) $(0)°_8$.

TABLE II Onset strains for transverse cracking, edge delamination and matrix microcracking under uniaxial tension of cross-ply SiC/CAS composites

Failure strain	Specimen lay-up			
	$(0)_8$	$0_3/90/0_3$	$0_3/90_2/0_3$	$0_3/90_3/0_3$
Transverse cracking (%)	–	0.05	0.025	0.012
Edge delamination (%)	–	0.06	0.06	0.06
Matrix microcracking (%)	0.13	0.13	0.13	0.13

initiated, immediately propagated through the matrix, while in the $0°_3/90°/0°_3$ composites, the crack propagation was delayed until a slightly higher strain was reached. When the cracks reached the 0° ply, they travelled only a few fibre spacings into the ply and then stopped by the fibres in the 0° ply. Similar to the matrix microcracks in the unidirectional composites, the transverse cracks were regularly spaced and their spacing decreased with increasing applied strain, Fig. 11.

The second failure event was the delamination cracking of the 90° ply which always appeared only after transverse cracking had occurred. The delamination cracks originated from voids between each pair of transverse cracks and subsequently travelled towards the two transverse cracks. With increasing composite strain, these cracks eventually coalesced into one long crack in the 90° ply along a zigzagged path. From the micrographs, it seemed that the delamination cracks only occurred inside the 90° ply away from the 0°/90° ply interface.

Specimens were sectioned to examine the delamination cracks transversely. The observations indicated that cracks started from both edges, apparently due to free-edge effects, and propagated towards the interior of the specimen.

As the composite strain reached 0.13%, which was the matrix cracking strain for the unidirectional composites, matrix microcracking in the 0° plies started for all three cross-ply laminates. The microcracks did not necessarily extend from the existing transverse ply cracks but often appeared first in the outer section of the 0° ply or within the matrix-rich regions. They then multiplied throughout the matrix as the strain increased. Most of the cracks stopped at the 0°/90° interface but some travelled further into the transverse ply at a higher strain and were finally arrested by the delamination cracks in the transverse ply. The composites eventually failed by fibre breakage with extensive fibre pull-out in the 0° ply.

Transverse cracks and matrix microcracks spacings as a function of composite strain are given in Figs 8 and 11, respectively. The transverse crack spacing is found to increase with increasing 90° ply thickness. The crack spacing first decreased sharply then seemed to have reached the limiting value before the start of the matrix microcracking; however, it decreased further when the matrix microcracks propagated into the transverse ply. Unlike the transverse cracks, matrix microcrack spacing was unaffected by the 90° ply thickness as shown in Fig. 8. This, together with the observation that matrix microcracking strain is the same in the unidirectional and cross-ply laminates, seems to indicate that 90° ply transverse cracking has

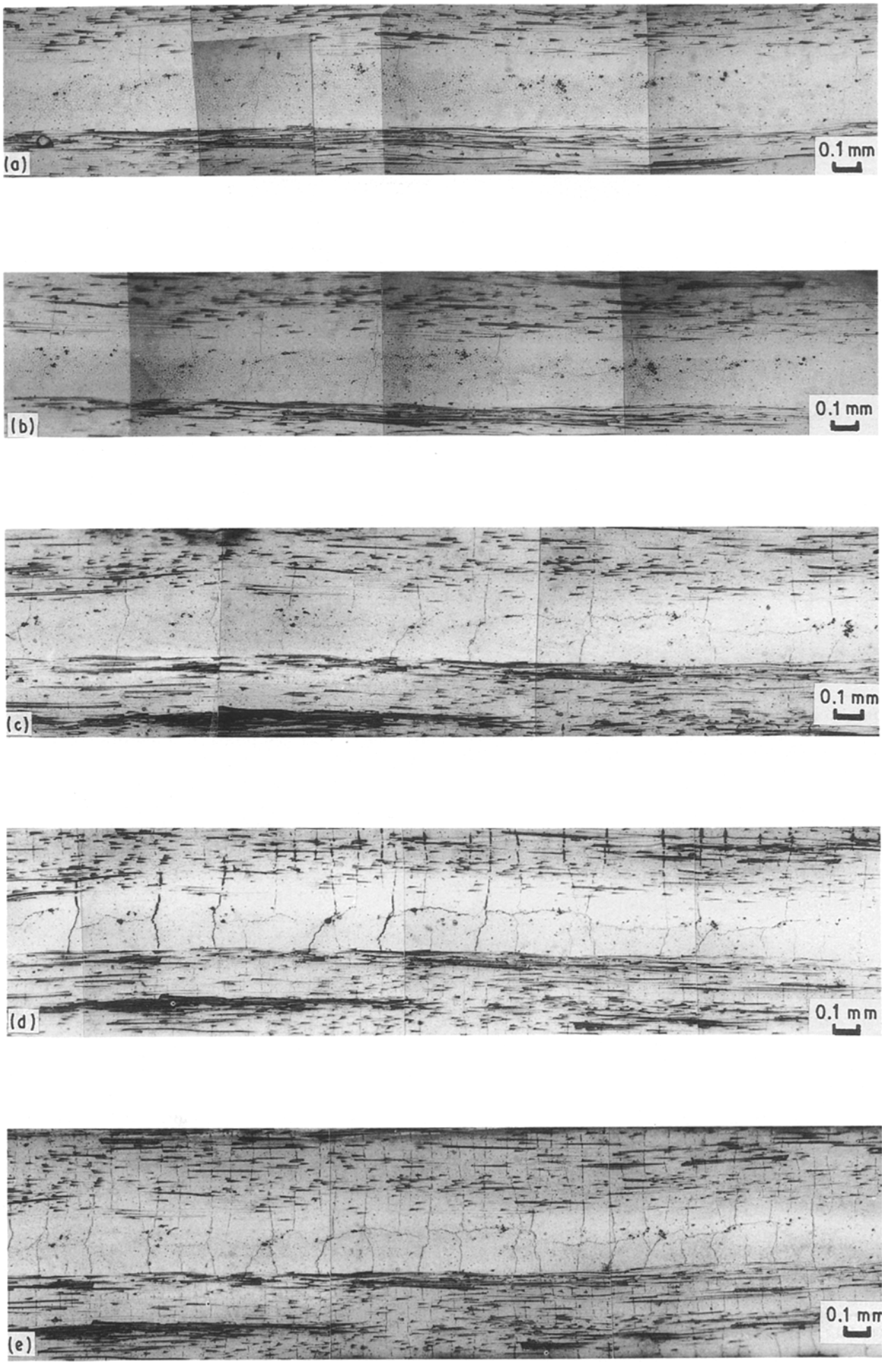

Figure 9 Micrographs obtained from replica tapes showing the sequence of the failure events in the $0°_3/90°/0°_3$ SiC/CAS laminate.

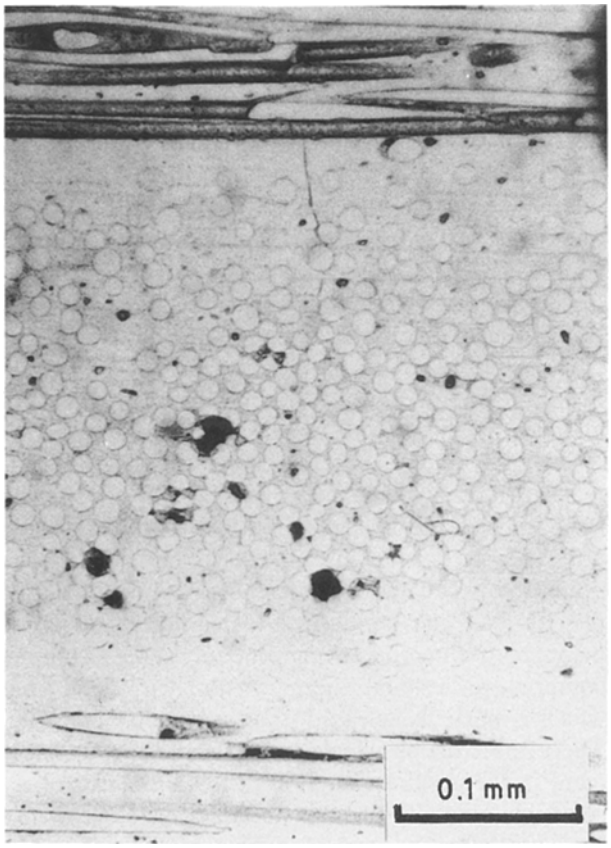

Figure 10 A transverse crack initiated at the 0°/90° ply interface.

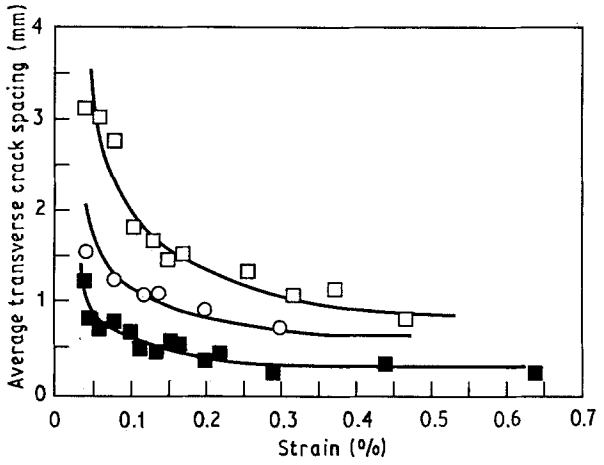

Figure 11 Average transverse crack spacing for SiC/CAS cross-ply laminates as a function of composite strain. (■) $0°_3/90°/0°_3$, (○) $0°_3/90°_2/0°_3$, (□) $0°_3/90°_3/0°_3$.

no effect on the 0° ply matrix cracking with the implication that the unidirectional laminates are notch-insensitive.

3.2. Tensile loading/unloading/reloading tests

Fig. 12 shows the tensile stress–strain curves for unidirectional, $0°_3/90°/0°_3$ and $0°_3/90°_3/0°_3$ cross-ply laminates under a series of incremental loading and unloading. The normalized stiffness reduction from each loading cycle as well as the associated crack density are shown in Figs 13 and 14.

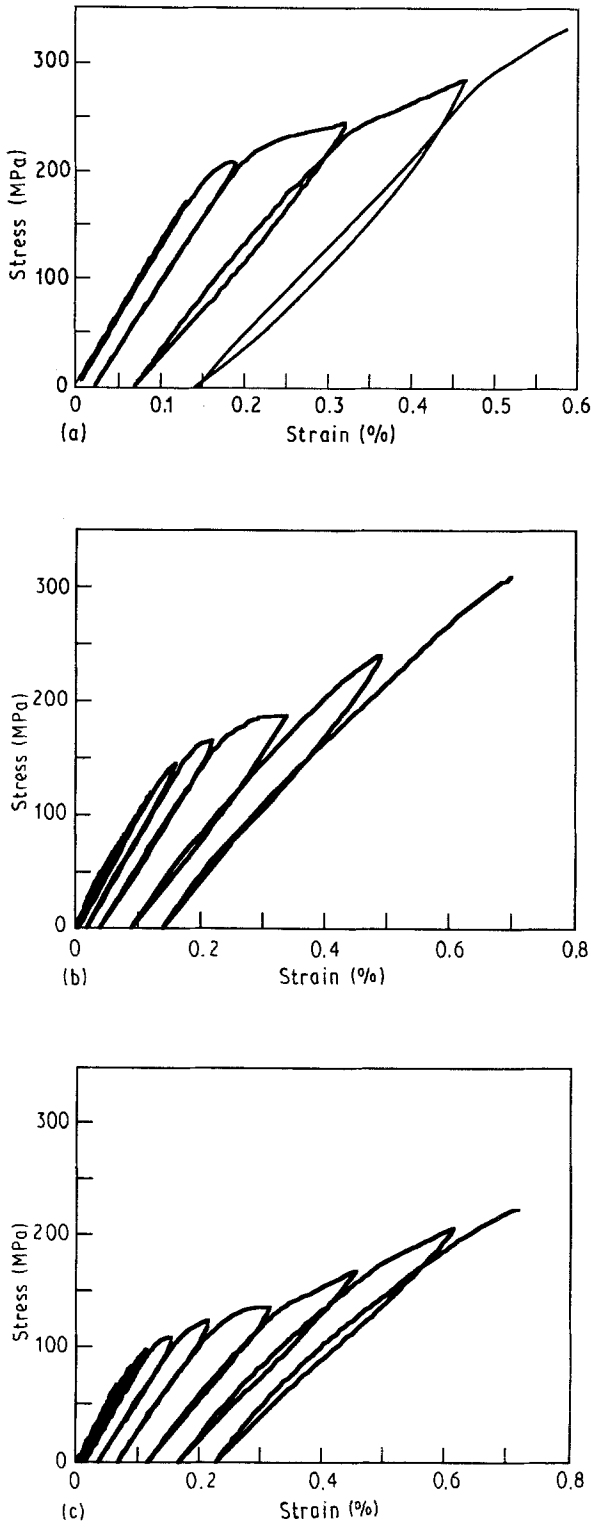

Figure 12 (a) Tensile stress–strain curves from cyclic loading of SiC/CAS unidirectional composite. (b) Tensile stress–strain curves from cyclic loading of $0°_3/90°/0°_3$ SiC/CAS laminate. (c) Tensile stress–strain curves from cyclic loading of $0°_3/90°_3/0°_3$ SiC/CAS laminate.

For the unidirectional laminate, the stiffness decreases as the matrix starts to crack, however, the effect is initially very small due to the very small number of cracks when cracking just starts. At the higher strain levels, the reduction in stiffness slows down as the matrix crack density reaches a relatively stable value. There is further decrease in stiffness near the end of the test which must be due to other failure mechanisms, such as fibre breakage as the process of matrix cracking has already been completed.

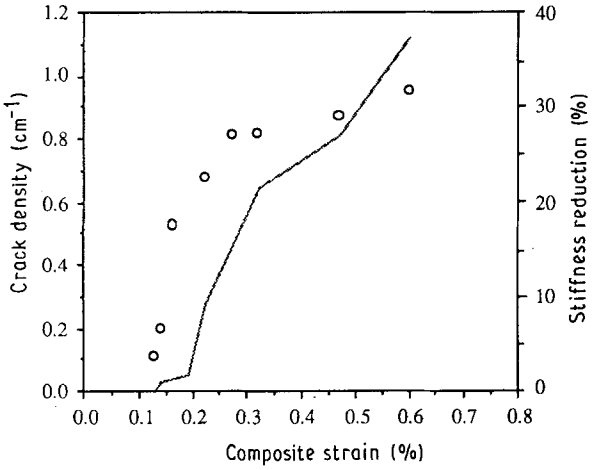

Figure 13 (∿∿∿) Stiffness reduction and (○) matrix crack density versus composite strain for a unidirectional SiC/CAS laminate subjected to incremental loading/unloading cycles.

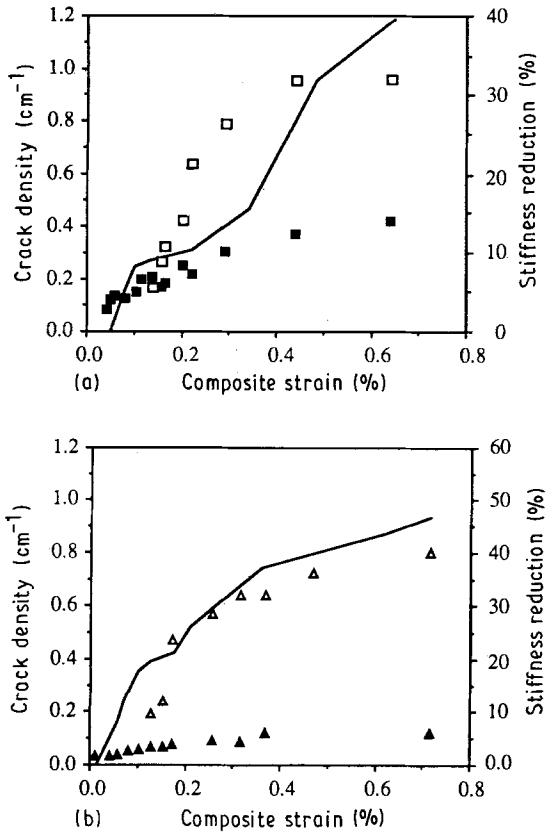

Figure 14 (——) Stiffness decrease and crack densities of (■, ▲) transverse cracks and (□, △) matrix microcracks versus strain for SiC/CAS laminates with ply sequence of (a) $0°_3/90°/0°_3$ and (b) $0°_3/90°_3/0°_3$.

The residual strain observed after each loading/unloading cycle indicates that matrix cracking has induced irreversible damage in the composite. Part of the residual strain could come from the release of the residual thermal stress in the fibre as the matrix cracks. Because the thermal expansion coefficient of the Nicalon fibre is smaller than that of the CAS matrix, the fibre in the composite is in compression in the axial direction. As the matrix cracks, fibres bridging the crack can release their residual thermal stress and extend between the crack surfaces.

For the cross-ply laminates, the stiffness starts to decrease as the transverse cracking initiates and the degree of this degradation is higher in the $0°_3/90°_3/0°_3$ laminate due to the thicker 90° ply. As illustrated in Fig. 14, good correlation exists between stiffness reduction and densities of transverse cracks and matrix microcracks. The rate of stiffness reduction slows down as transverse cracking approaches its saturation state while at the same time matrix microcracking is just emerging. A dramatic drop in the stiffness occurs just prior to the final failure after both types of crackings have already been fully developed. This late drop is believed to have been due to fibre breakage, as also seen in the unidirectional composite.

As in the unidirectional laminate, each loading/unloading loop displayed a hysteresis in strain. The magnitude of the hysteresis was initially small when only transverse cracking was occurring but became noticeable when the matrix microcracking in the 0° ply started. The permanent displacement observed before matrix microcracking probably results from the compressive residual thermal strain in the 0° ply which is partially released upon transverse cracking. The same reasons which yield permanent displacement in the unidirectional SiC/CAS laminate are responsible for the hysteresis observed in the cross-ply laminates after the start of matrix cracking.

The fracture toughness determinations from the chevron-notched specimens of the unidirectional composites yielded a K_c of 1.52 ± 0.05 MN m$^{-3/2}$ for a crack propagating parallel to the fibre axis. The work of fracture calculated is 9.86 J m^{-2}.

From the thermomechanical experiments, the strain-free temperature for the SiC/CAS composite system was assessed to be 600 °C. The thermal expansion coefficients obtained from room temperature to 600 °C were 4.28 μm m^{-1} °C^{-1} for the longitudinal direction, α_l, and 5.25 μm m^{-1} °C^{-1} for the transverse direction, α_t.

4. Discussion

4.1. Unidirectional SiC/CAS composites

Although *in situ* microscopy clearly showed that matrix cracks initiated at an axial strain of about 0.13%, the stress–strain curve did not indicate any deviation from linearity until it reached a higher strain. This is because the matrix cracks, when just initiated, are confined to a small area; the length of these cracks is in the neighbourhood of several fibre spacings at most and none travels immediately through the whole width of the specimen. Therefore, their effect on the stress–strain behaviour at the onset strain level is limited. Moreover, the strain gauge only covers a small section of the gauge length and, unless first matrix microcracks occur within the length covered by the strain gauge, it cannot detect the onset of cracking. The strain gauge sensitivity can be increased by using a short gauge length. However, because the deformation field in a damaged composite is inhomogeneous, a displacement measurement made over a larger test section characterizes the laminate response better than one made over a smaller section.

Therefore, the tensile stress–strain curve cannot be used as a reliable indication of initiation of matrix cracks in this composite.

The reversal in the transverse strain near the proportional limit, which has been observed in other ceramic matrix composite systems [20], is believed to be due to the occurrence of matrix microcracks. When cracking occurs, the matrix tends to unload at and near the crack surfaces, thus reducing its lateral Poisson's contraction. As the number of matrix cracks increases, the contribution from the stress relief at the crack surfaces also increases. Therefore, the positive change in the transverse strain is more profound at higher applied stresses because of the increasing number of cracks. Eventually, when the matrix saturates with cracks, the transverse strain also reaches a limiting value, as observed from the experiments.

In addition, the matrix in the as-pressed composite is in tension along the fibre direction because of the mismatch in the coefficients of thermal expansion of the matrix and the fibre. The debonding of the fibre/matrix interface at the crack tip uncouples the fibres and the matrix, thus relieving this residual thermal stress and the associated Poisson's contraction. This could explain the positive reading of the transverse strain near the end of the microcracking process.

The crack spacing at failure can be used to calculate the interfacial frictional strength, τ, from Aveston *et al.*'s model [6]. It has been shown [21] that the measured mean crack spacing, x', is about 1.34 times the limiting crack spacing, x. The interfacial strength thus calculated is 14.4 MPa. This value agrees very well with the interfacial strength averaging 13.7 MPa obtained by the authors using various indentation techniques.

The matrix cracking strain, ε_{muc}, calculated from Aveston *et al.*'s theory is 0.24%. This is high when compared to the experimental value of 0.13% which is just slightly larger than the ultimate tensile strain of the bulk matrix material. There are several reasons for the lower than predicted values for the matrix cracking strain. Matrix-rich regions, some as wide as several hundred micrometres, have been observed quite often between the individual plies in the unidirectional laminates. This translates into very low local fibre volume fraction and therefore a matrix response that is not too different from that of the bulk matrix. However although the nonuniformity in fibre distribution could account for the early appearance of the matrix cracks observed in the matrix-rich regions, cracks multiplied rapidly throughout the rest of the matrix immediately following their first occurrence. It therefore appears that the theoretical overestimation must be due to other sources.

Part of the discrepancy could be due to the residual tensile stress in the matrix resulting from the mismatch of thermal expansion coefficients between the fibre and the matrix ($\alpha_m = 5.0\ \mu m\ m^{-1}\ °C^{-1}$ and $\alpha_f = 4\ \mu m\ m^{-1}\ °C^{-1}$). This residual thermal stress, which is not considered in Aveston *et al.*'s model is, however, only of the order of 0.04%. Another source for the difference could be in using the fracture toughness of the bulk CAS in the calculation. The properties of the matrix in the SiC/CAS may differ significantly because the pressure and the heat-treatment history experienced by the CAS in the composite are quite different from those experienced by the monolithic CAS material. Also, it has been reported that crystal growth of the anorthite in the CAS could depend on the fibre arrangement [22]. Therefore, the value of $2.2\ MN\ m^{-3/2}$ used here probably overestimates the actual toughness of CAS in the composites and, in turn, the predicted value of the matrix cracking strain.

4.2. 0,90,0 Cross-ply laminates

The failure events occurred in the cross-ply laminates in the following sequence: (a) transverse cracking, (b) delamination cracking, and (c) matrix microcracking.

4.2.1. Transverse cracking

From the results of the thermomechanical analysis of the SiC/CAS unidirectional composite, it is obvious that there would be processing-induced residual thermal stresses in the cross-ply laminates. Of special interest is the axial stress in the longitudinal and the transverse plies. According to the classical laminated plate theory, this thermally induced in-plane normal stress, σ_x, should be a uniform tension in the 90° ply and a uniform compression in the 0° ply. However, when an edge effect is included in the analysis, the stress field near the laminate-free surfaces becomes complex. Theoretical calculations [23] using a finite-element procedure with an advanced sparse matrix solution technique on a similar composite lay-up, indicate that in the 90° ply σ_x has its maximum tensile value near the ply interface and gradually falls off to its nominal value, which is induced by the temperature change during processing, toward the centre of the ply. In the 0° ply, maximum compressive stress similarly occurs near the ply interface and then drops down to its nominal value at the free, outer surface of the ply. This residual stress distribution therefore accounts for the observed initiation of the transverse cracks at the ply interface. However, the experimental observations were limited to the free surface. No information of the initiation of the transverse cracks inside the specimen was available.

Fig. 15 shows a plot of the onset strain for transverse cracking as a function of the inner ply thickness, $2d$. Also shown are the theoretical minimum transverse cracking strains calculated from the transverse cracking analyses of Bailey *et al.* [10], taking a ΔT of 575 °C (the strain-free temperature for the SiC/CAS composites was experimentally determined as 600 °C). An experimental value of $9.86\ J\ m^{-2}$ is used for γ_t. Fig. 15 also depicts the theoretical calculations from the simple constraint theory where the residual thermal strain [9] is neglected. Clearly, the residual thermal strain in the 90° ply plays an important role in the onset strain for transverse cracking. In the absence of the residual strain, a higher onset strain for all cross-ply laminates and a greater difference between the cracking strain of the three laminates would have been obtained. Because this residual strain increased with

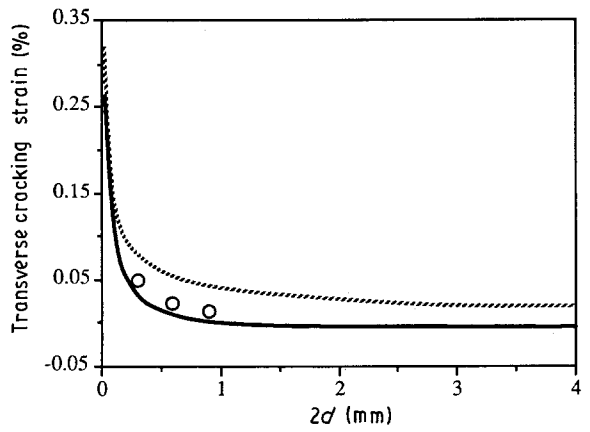

Figure 15 Onset transverse cracking strain as a function of the 90° ply thickness, 2*d*.

decreasing 90° ply thickness, the observed difference in the onset strain of the three cross-ply laminates was smaller than the actual difference.

The strain at which first transverse cracking occurs depends, in general, on the thickness of the 90° ply because of two effects. The first one is the thickness effect due to the flaw distribution. From the statistical point of view, the thinner the 90° ply, the smaller the probability of a strength-controlling flaw, and, therefore, the higher the ply strength and strain-to-failure. The other is the constraint effect from the stiffer outer plies which increases the transverse ply failure strain, as analysed by Bailey *et al.* [10]. The thinner the 90° ply, the greater is the constraint effect and, therefore, the higher the transverse cracking strain. In addition to the thickness of the 90° ply, this effect also depends on the ratio of the Young's moduli of the 0° and the 90° plies. The higher the ratio, that is, the stiffer the 0° ply, the larger is the constraint effect. Therefore, in the SiC/CAS composite system where the E_l/E_t ratio is small, the magnitude of the constraint effect is not expected to be significant. The residual thermal strain which is higher for the laminate with thinner 90° ply makes this constraint effect even less obvious. However, from the close match between the experimental data and the theoretical predictions, as shown in Fig. 15, and the observation that transverse cracks propagated in two steps in the $0°_3/90°/0°_3$ laminate, the constrain effect does exist and contributes to the variation of the onset strain for transverse cracking with the 90° ply thickness.

From the above discussion, therefore, it appears that the variation in the transverse cracking strain as a function of the 90° ply thickness is due to both the statistical flaw distribution and the constraint effect.

4.2.2. Delamination cracking

The delamination cracks in the transverse ply are believed to result primarily from the free-edge effect which is, in turn, caused by transverse cracking. The magnitude of the out-of-plane interlaminar stresses induced by edge effect for a certain ply lay-up such as 0,90,0, greatly depend on the ply properties. The most controlling one is the mismatch in the Poisson's ratios of plies of different fibre orientations: the larger the mismatch the higher the magnitude of these interlaminar stresses. However, the Poisson's ratios for a unidirectional SiC/CAS laminate in the longitudinal and transverse direction (0.29 and 0.27, respectively) are very close to each other. That is, if the ply properties remain unchanged during loading, edge delamination should never take place. However, the experimental observations indicated that transverse cracking always preceded edge delamination which is an indication that transverse cracking changes the ply properties, thus contributing to the local initiation as well as the propagation of the delamination cracks. Transverse cracking not only releases most of the thermal residual stress, it also considerably reduces the stiffness and the Poisson's ratio of the 90° ply.

Microscopically, when a transverse crack forms, a region of the 90° ply on either side of the crack unloads. This unloading tends to release the Poisson's contraction of the 90° ply in the thickness direction as well as in the width direction near the crack. The relaxation of the 90° ply, however, is inhibited by the outer 0° plies in both directions. Especially in the width direction, the Poisson's contraction of the locally overloaded 0° plies near the crack is resisted by the high-modulus Nicalon fibres in the 90° ply. However, away from the cracks, both 0° and 90° ply contract accordingly because of their similar values in the Poisson's ratio. As a result, local tensile stresses develop in the 90° ply near the transverse cracks along the thickness direction to open up the 90° ply to accommodate the inhibited Poisson's contraction in the width direction. This tensile stress has its maximum near the cracks and is minimum in the region between the cracks. The local delamination originates from defects in the 90° ply near the cracks where the tensile stress due to the Poisson's effect is at a maximum.

As the composite strain increases, more and more transverse cracks occur. This increases the number of initiation sites for the delamination cracks and, in the meantime, the earlier initiated ones propagate longitudinally and coalesce to form a macroscopic delamination crack which then travels into the laminate.

Macroscopically, the occurrence of the transverse cracks greatly diminishes the stiffness and Poisson's ratio of the 90° ply in the loading direction. The cracked 90° ply can, therefore, be viewed as a physically sound ply but with reduced properties. This results in a large Poisson's ratio mismatch (0.29 for the 0° ply compared to 0 for the 90° ply) needed for edge delamination to occur. Therefore, transverse cracking is liable for the initiation of edge delaminations in the SiC/CAS 0,90,0 cross-ply laminates.

This experimental observation of the occurrence and the location of edge delamination has been confirmed by the analytical predictions of Wang's model [13]. Using fracture mechanics approach coupled with a three-dimensional finite element procedure, the results for the onset strain as well as the possible locations of this free-edge delamination are reported in a separate publication.

4.2.3. Matrix microcracking

The 0° plies appeared to be insensitive to the transverse cracking. They behaved identically to the unidirectional composites in terms of their microcracking strain and spacing despite the fact that the transverse cracks had propagated into these plies a few fibre diameters. They spill of transverse cracks into the 0 plies is most likely due to the kinetic energy of the cracks. The fracture mechanics analysis of Marshall *et al.* [24] shows that for a unidirectional composite, the matrix cracking stress approaches a steady-state value for crack lengths greater than $c_m/3$, where

$$c_m = \left(\frac{\pi}{4I^{4/3}}\right)\left[\frac{K_c^M E_m V_m^2(1+\eta)r(1-\nu^2)}{\tau V_f^2 E_f}\right]^{2/3} \quad (1)$$

where K_c^M is the critical stress intensity factor for the matrix, I is a dimensionless crack geometry constant and equals 1.2 for straight cracks, and $\eta = E_f V_f/E_m V_m$. Their analysis suggests that the stress for matrix cracking becomes independent of the length of matrix cracks or flaws as long as these flaws are over $c_m/3$. For SiC/CAS composites, the calculated critical crack length, $c_m/3$, is only 49 μm which is very close to the distance of transverse crack extension into the 0° plies. The above observations, therefore, could only be made if the 0° plies and the unidirectional composites contained pre-existing matrix flaws equal to or greater than the critical length.

4.3. Stiffness degradation during tensile loading

Simple calculations were made to provide upper and lower bounds for the variation of the composite stiffness as a function of the composite strain. For the unidirectional laminates, an upper bound was based on the assumption that the fibre/matrix interface was fully bonded. The lower bound was obtained by assuming that the fibre/matrix interface was purely frictional and the load transfer between the fibre and the fragmented matrix was through a constant shear stress.

4.3.1. Unidirectional laminates

4.3.1.1. Bonded fibre/matrix interface. Based on the assumption that the fibre/matrix is fully bonded, an upper bound is derived from the shear lag model of Aveston and Kelly [25]. They consider that in the plane of the first crack the fibres will be subjected to an additional stress, $\Delta\sigma_0$, where

$$\Delta\sigma_0 = \frac{\sigma_a}{V_f} - \varepsilon_{mu} E_f \quad (2)$$

where σ_a is the applied stress, ε_{mu} is the matrix cracking strain, and E_f and V_f are the Young's modulus and the volume fraction of the fibre, respectively. This additional stress then decays with the distance y from the crack surface. From a modified shear lag analysis, the distribution of this additional stress, $\Delta\sigma$, in the fibre is given by

$$\Delta\sigma = \Delta\sigma_0 \exp(-\phi^{1/2} y) \quad (3)$$

where ϕ can be calculated from

$$\phi = \left(\frac{2G_m E_c}{E_f E_m V_m}\right)\frac{1}{r^2[\ln(R/r)]} \quad (4)$$

where G_m is the shear modulus of the matrix, E_c is the initial composite Young's modulus, E_m and V_m are the Young's modulus and the volume fraction of the matrix, respectively, R is half of the distance between the centres of two adjacent fibres and r is the fibre radius. In the calculation, a value of 12.5 μm, which is estimated based on a fibre volume fraction of 0.36, is used for R.

The stress distribution in the matrix is therefore given by

$$\sigma_m(y) = \varepsilon_{mu} E_m - \Delta\sigma \frac{V_f}{V_m} \quad (5)$$

Rearranging Equation 5 gives

$$E_m(y) = E_m - E_m \exp(-\phi^{1/2} y) \quad (6)$$

For a matrix crack spacing, s, the effective stiffness of the matrix is obtained by averaging $E_m(y)$ over s

$$\bar{E}_m = \left(2\int_0^{s/2} E_m \mathrm{d}y\right) \Big/ \left(2\int_0^{s/2} \mathrm{d}y\right) \quad (7)$$

The average value of the stiffness in the matrix is therefore given by

$$\bar{E}_m = E_m + \frac{2E_m}{\phi^{1/2} s}\left[\exp\left(-\phi^{1/2}\frac{s}{2}\right) - 1\right] \quad (8)$$

The stiffness of the unidirectional composite is then calculated following the rule of mixtures

$$E_1 = \bar{E}_m V_m + E_f V_f \quad (9)$$

4.3.1.2. Frictional fibre/matrix interface. With the assumption that the fibre/matrix interface is frictional, the load transfer between fibre and matrix is constant. After the matrix cracking has occurred, the additional stress transferred to the fibre at the crack surface should be transferred back to the matrix by a constant interfacial shear stress over the distance of the limiting matrix crack spacing, x. The stress in the matrix away from the crack surface will therefore vary linearly, between zero at the crack and a maximum of σ_m at a distance x from the crack. This stress will stay at its maximum level for distances longer than x. The average stress and the stiffness values in the matrix can therefore be represented by the following equations

$$\bar{\sigma}_m = \frac{\sigma_m(s-x)}{s} \quad (10)$$

$$\bar{E}_m = E_m \frac{s-x}{s} \quad (11)$$

The composite stiffness is then calculated from Equation 9. In the calculation, a value of 105 μm, which is matrix crack spacing measured from the experiments divided by 1.34 [21], is used for x.

4.3.2. Cross-ply laminates

A first-order approximation of the stiffness degradation under tensile loading, similar to that conducted for the unidirectional composite, is carried out for the 0,90,0 cross-ply laminates. Because delamination between the 0° and the 90° ply has never been observed, only a perfectly bonded case is considered. The distribution of the apparent stiffness of a segment of a 90° ply between the two transverse crack surfaces is calculated based on the result from the modified shear lag analysis [8]. From the relationship between the crack spacing and the composite strain, the average stiffness of the fragmented 90° ply is obtained as a function of the composite strain. The composite stiffness is then calculated from the rule of mixtures, using the initial stiffness of the 0° ply prior to matrix microcracking and the reduced 0° ply stiffness after the matrix microcracking. The consideration of either a fully bonded or a frictional interface between the fibre and the matrix in the calculation of the reduced stiffness of the 0° ply led to upper and lower bounds for the reduced stiffness in the cross-ply laminate.

Based on the shear lag analysis of Garrett and Bailey [8], an additional stress, $\Delta\sigma$, is thrown on to the outer 0° plies when a crack occurs in the 90° ply at a strain of ε_{tu}; $\Delta\sigma$ is given by

$$\Delta\sigma = \frac{d}{b}\varepsilon_{tu}E_t\exp(-\phi_t^{1/2}y) \quad (12)$$

where b is the 0° ply thickness, d is the half thickness of the 90° ply, E_t is the modulus of the 90° ply, E_l is the modulus of the 0° ply, y is the distance from the plane of the crack along the length of the specimen. ϕ_t in Equation 12 is given by

$$\phi_t = \frac{E_c G_t}{E_l E_t}\frac{b+d}{bd^2} \quad (13)$$

where E_c is the initial modulus of the cross-ply laminate, and G_t the shear modulus of the 90° ply parallel to the fibres.

The stress distribution in a fragment of the cracked 90° ply is thus given by

$$\sigma_t(y) = \varepsilon_{tu}E_t - \varepsilon_{tu}E_t\exp(-\phi_t^{1/2}y) \quad (14)$$

The associated apparent modulus is thus expressed by

$$E_t(y) = E_t - E_t\exp(-\phi_t^{1/2}y) \quad (15)$$

Averaging over the distance between the two crack surfaces, l, gives

$$\bar{E}_t = 2\int_0^{l/2} E_t\,dy/2\int_0^{l/2} dy \quad (16)$$

which yields

$$\bar{E}_t = E_t + \frac{2E_t}{\phi_t^{1/2}l}\left[\exp\left(-\phi_t^{1/2}\frac{l}{2}\right) - 1\right] \quad (17)$$

The stiffness of the laminate is calculated from

$$\bar{E}_c = E_l\frac{b}{b+d} + \bar{E}_t\frac{d}{b+d} \quad (18)$$

prior to matrix microcracking in the 0° ply, and

$$\bar{E}_c = \bar{E}_l\frac{b}{b+d} + \bar{E}_t\frac{d}{b+d} \quad (19)$$

after matrix microcracking. $\bar{E}_l$ is calculated using Equation 9 with $\bar{E}_m$ obtained either from Equation 8 for a fully bonded fibre/matrix interface or Equation 11 for a frictional interface.

Results from the calculation are shown in Figs 15 and 16 for unidirectional and cross-ply laminates, respectively. They are depicted as a function of composite strain using the experimentally obtained relation between the crack spacing and the composite strain. The stiffness reduction is calculated up to a

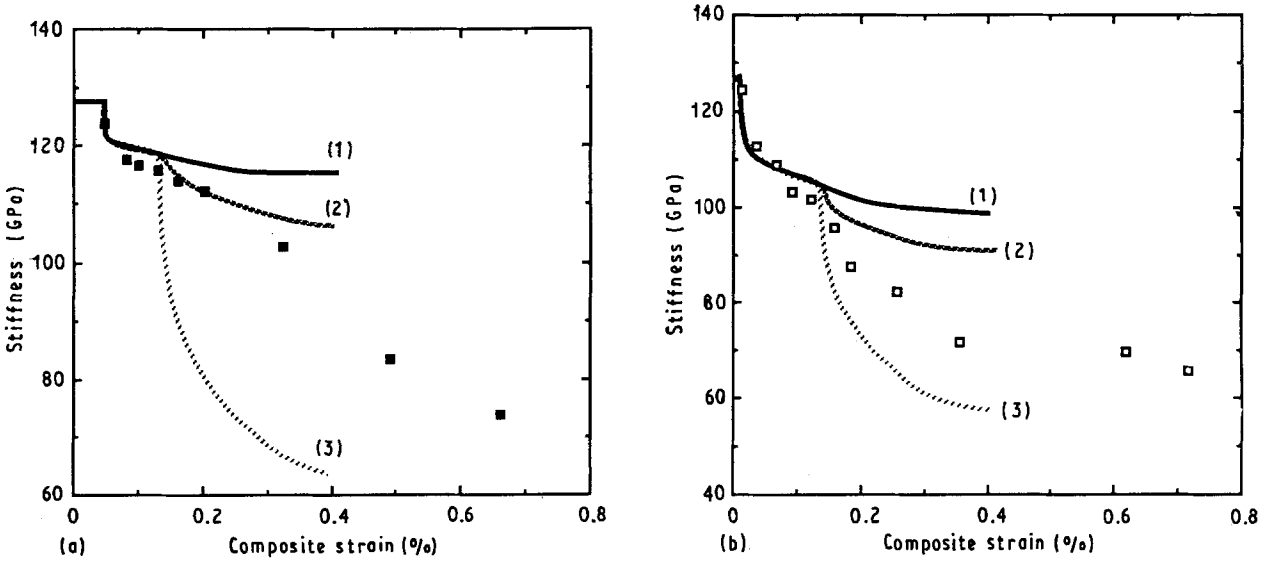

Figure 16 Stiffness reduction as a function of the composite strain for the SiC/CAS (a) $0°_3/90°/0°_3$ and (b) $0°_3/90°_3/0°_3$ laminates. 1, Theoretical predictions for the laminate showing only transverse cracking. 2, Theoretical predictions for the laminate with transverse cracks plus matrix microcracks (fully bonded interface). 3, Theoretical predictions for the laminate with transverse cracks plus matrix microcracks. (□, ■) Experimental data.

composite strain of only 0.4%, because at higher strain other failure modes besides matrix cracking in the unidirectional laminates, and transverse cracking plus matrix cracking in the cross-ply laminates may occur and invalidate the above simple analysis. Also included in these figures are the experimental data.

For the unidirectional laminates, as seen in Fig. 15, the experimental data are bounded by the theoretical predictions made with the two types of interface. Initially, the experimental data are closer to the predictions based on a bonded interface. However, at higher strain levels, they become closer to the predictions assuming a frictional interface. This comparison made between the theoretical predictions and the experimental data may imply that the bonding between the fibre and matrix in the as-processed SiC/CAS composite is not purely frictional. It is likely that a chemical bond initially exists at the fibre/matrix interface. However, this chemical bond is weak and is readily destroyed after matrix cracks start to appear. As a result, at higher strain levels, the load transfer is through a constant interfacial frictional stress and is therefore much less efficient.

For the $0°_3/90°/0°_3$ and the $0°_3/90°_3/0°_3$ laminates, it seems that the stiffness reduction resulting from transverse cracking matches the theoretical predictions well. Again, as in the case of the unidirectional composite, the composite stiffness after the occurrence of matrix microcracking fell in between the predictions for the fully bonded and for the frictional fiber/matrix interfaces. This observation once again supports the hypothesis presented above that there might exist a weak chemical bonding between the carbon-rich layer and the CAS matrix, which is gradually destroyed after the matrix starts cracking.

5. Conclusions

1. The stress–strain behaviour of the SiC/CAS unidirectional composites and cross-ply laminates were determined under tensile loading using a especially designed end-tabbed test coupon.

2. In unidirectional composites subjected to tensile loading along the fibre direction, matrix cracking is the first damage event to appear. The number of cracks increases rapidly and reaches a saturation level. Fibre breakage appears occasionally when matrix cracking is approaching its saturation point and peaks at the final failure, beyond which considerable fibre pull-out ensues.

3. The sequence of failure events in the cross-ply laminates was (1) transverse and (2) delamination cracking in the 90° ply, and (3) matrix microcracking in the 0° ply.

4. The strain at which transverse cracking commenced increased with decreasing 90° ply thickness in 0°,90°,0° cross-ply laminates in agreement with the crack constraining theory.

5. Transverse cracking caused the occurrence of delamination cracks in the 90° ply by reducing the Poisson's contraction in the fractured 90° segments and enhancing the edge interlaminar stress.

6. The matrix cracking strain and the average matrix crack spacing of the 0° ply in the cross-ply laminate were not affected by the cracking in the 90° ply.

7. The comparison made between the theoretical approximations of the stiffness reduction and the experimental data from the incremental cyclic loading test implies that a weak chemical bond may initially exist between the fibre and the matrix which may be subsequently destroyed when matrix cracking starts.

Acknowledgements

The authors thank the Air Force Office of Scientific Research (Dr Liselotte J. Schioler, Program Monitor) and the Center for Composite Materials, University of Delaware, for their support of this work. Appreciation is extended gratefully to Professor A. S. D. Wang for many valuable discussions.

References

1. L. J. SCHIOLER and J. J. STIGLICH, *Amer. Ceram. Soc. Bull.* **65** (1986) 289.
2. K. PREWO, J. J. BRENNAN and G. K. LAYDEN, *ibid.* **65** (1986) 305.
3. G. A. COOPER and J. M. SILLWOOD, *J. Mater. Sci.* **7** (1972) 325.
4. D. B. MARSHALL and A. G. EVANS, *J. Amer. Ceram. Soc.* **68** (1985) 225.
5. R. T. BHATT and R. E. PHILLIPS, *J. Comp. Tech. Res.* **12** (1990) 13.
6. J. AVESTON, G. A. COOPER and A. KELLY, in "Proceeding of the Conference on Properties of Fiber Composites", National Physical Laboratory (Guildford IPC Science and Technology Press, Surrey, 1971) p. 15.
7. J. AVESTON and A. KELLY, *J. Mater. Sci.* **8** (1973) 352.
8. K. W. GARRETT and J. E. BAILEY, *ibid.* **12** (1977) 157.
9. A. PARVIZI, K. W. GARRETT and J. E. BAILEY, *ibid.* **13** (1978) 195.
10. J. E. BAILEY, P. T. CURTIS and A. PARVIZI, *Proc. R. Soc. Lond. A.* **366** (1979) 599.
11. R. B. PIPES and N. J. PAGANO, *J. Compos. Mater.* **4** (1970) 538.
12. D. J. WILKINS, J. R. EISENMANN, R. A. CAMIN, W. S. MARGOLIS and R. A. BENSON, in "Damage in Composite Materials", edited by K. L. Reifsnider, ASTM STP 775 (American Society for Testing and Materials, Philadelphia, PA, 1982) p. 168.
13. A. S. D. WANG, in "Interlaminar Responses in Composite Laminates", edited by N. J. Pagano (Elsevier Applied Science, 1989) pp. 69–108.
14. S. R. SONI and R. Y. KIM, in "Composite Materials: Testing and Design", ASTM STP 893, edited by J. M. Whitney (American Society for Testing and Materials, Philadelphia, PA, 1986) p. 287.
15. A. S. D. WANG and F. W. CROSSMAN, *J. Compos. Mater. Suppl.* **14** (1980) 71.
16. *Idem., ibid.* **14** (1980) 88.
17. F. W. CROSSMAN and A. S. D. WANG, in "Damages in Composite Materials", edited by K. L. Reifsnider, ASTM STP 775 (American Society for Testing and Materials, Philadelphia, PA, 1982) p. 118.
18. J. I. BLUHM, *Engng Fract. Mech.* **7** (1975) 593.
19. *Idem.*, in "Fracture", Vol. 3, edited by D. M. R. Taplin (University of Waterloo Press, Waterloo, Ontario, Canada, 1977) p. 409.

20. R. Y. KIM and A. P. KATZ, *Ceram. Engng Sci. Proc.* **9** (1988) 853.
21. A. C. KIMBER and J. G. KEER, *J. Mater. Sci. Lett.* **1** (1982) 353.
22. J. ADAMS, in "92nd Annual Meeting of the American Ceramic Society", Dallas, Texas, April 1990.
23. A. S. D. WANG and F. W. CROSSMAN, *J. Compos. Mater.* **11** (1977) 300.
24. D. B. MARSHALL, B. N. COX and A. G. EVANS, *Acta Metall.* **23** (1985) 2013.
25. J. AVESTON and A. KELLY, *J. Mater. Sci.* **8** (1973) 352.

Received 19 June
and accepted 12 September 1991